EVALUATING ECOGEOGRAPHIC VARIATION IN HUMAN NASAL PASSAGES USING IN-SILICO DECONGESTION OF THE NASAL CYCLE

INTERNSHIP PRACTICUM REPORT

Presented to the Graduate Council of the

Graduate School of Biomedical Sciences at

University of North Texas

Health Science Center at Fort Worth

in Partial Fulfillment of the Requirements

For the Degree of

MASTER OF SCIENCE

By

Elizabeth Thai, B.S.

Fort Worth, Texas

May 2020

ACKNOWLEDGEMENTS

First and foremost, I want to thank my major professor, Dr. Scott D. Maddux, for his guidance and support throughout the course of my work. As my mentor, he has helped me grow in more ways than I could ever give him credit for here. Without him, this practicum would not have been possible.

I would like to extend my thanks to my collaborators Dr. Brian Dennis, Dr. Sandeep Patil and Hasintha Amaranayaka at the University of Texas at Arlington. Their contributions, patience, and expertise continue to be invaluable. I am most grateful to Dr. Todd Yokley at the Metropolitan State University of Denver for graciously providing me the samples used in my practicum.

I would like to thank the Graduate School of Biomedical Sciences at the University of North Texas Health Science Center for the opportunity to achieve this graduate degree. I would also like to express my gratitude to my committee members, Dr. Rachel Menegaz and Dr. Armando Rosales, for your advice and guidance throughout my practicum. To the individuals in the Center for Anatomical Sciences, Drs. Rustin Reeves, Rehana Lovely, Cara Fisher, Emma Wood, and my fellow student colleagues, thanks for your support. A special thanks to Ashley Steele and Suhhyun (Sarah) Kim for your unyielding encouragement, support, and inspiration. You've pushed me to realize my full potential as a scientist and as a person. I thank you both for believing in me.

Finally, to my partner, Jake Paireepinart, for providing me with unconditional love and support which has helped me turn my dreams into reality. My accomplishments are as much yours as they are mine. Thank you.

TABLE OF CONTENTS

LIST OF TABLES

LIST OF ILLUSTRATIONS

CHAPTER I

INTRODUCTION TO THE STUDY

The following practicum report was performed as a requirement for the Master of Science in Medical Sciences Anatomy Track program, from May 2019-May 2020, at the University of North Texas Health Science Center (UNTHSC). The study was conducted under the direct supervision of Scott Maddux, Ph.D., in the Center for Anatomical Sciences and Department of Physiology and Anatomy at UNTHSC.

The human nose is an anatomically complex structure that performs numerous functions including oxygen supply, olfaction, and the conditioning (filtering, warming, and humidifying) of inspired air. There is considerable variation in the morphology and physiological processes of the human nose both within, as well as across, populations (Franciscus and Long 1991). Since the demand for air conditioning is largely dependent on the external environment, many studies have found potential ecogeographic associations between nasal morphology and climate (Yokley 2009, Noback, Harvati et al. 2011, Butaric and Maddux 2016, Maddux, Butaric et al. 2017, Zaidi, Mattern et al. 2017, Marks, Maddux et al. 2019). More recently, computational fluid dynamics (CFD) analysis has been performed in an attempt to understand how air flows through the nose. However recent studies have cited limitations to CFD studies, including the nasal cycle and nasal congestion.

The focus of this practicum was the development of a methodology for creating realistic 3D models of the airway using computed tomography (CT) scans and 3D Slicer software (Fedorov,

Beichel et al. 2012). More specifically, this methodology accounts for the varied mucosal congestion of subjects during scanning to allow modeling of a fully decongested nose in all individuals. These methods are being actively employed to quantify the nasal cavity morphologies of subjects of European and African ancestral backgrounds. The models and methods developed in this practicum are also being utilized to generate 3D models of the nasal cavity for CFD analysis in conjunction with our collaborators at Dennis lab at the University of Texas at Arlington.

BACKGROUND AND LITERATURE

Section 1: Function of the Nose

The nose is a complex structure with numerous functions including oxygen supply, olfaction, and conditioning of inspired air. To protect the lungs, inspired air must be heated to body temperature (37 º C) and 100% saturated with water vapor by the time it reaches the lungs (Mygind and Dahl 1998). The majority of air conditioning happens in the nasal cavity with the nasal mucosa acting as the source of heat and moisture. As air passes through the nasal cavity, heat and moisture are transferred from the nasal mucosa to the air via concurrent convection and evaporation. During exhalation, the opposite happens and the nose recovers some heat and water from expired air (Walker and Wells Jr 1961). Previous studies have shown that variation in nasal anatomy impacts air conditioning capacity (Churchill, Shackelford et al. 2004, Naftali, Rosenfeld et al. 2005).

Section 2: Anatomy of the Nose

The nasal cavity communicates with the external environment via anterior apertures, nares, and nasopharynx via the posteriorly located choanae. The cavity is divided into two distinct airways by the nasal septum (Mygind and Dahl 1998). The nasal airways are comprised of the

external nose and the nasal cavity proper. The external nose includes the nasal vestibule and is covered by keratinized stratified squamous epithelium that minimally contributes to the conditioning of air. The nasal cavity proper is also known as the functional area and contains the olfactory and respiratory regions. The superior one third is covered with olfactory epithelium and the inferior two-thirds is covered with respiratory epithelium, which plays a major role in air conditioning.

The respiratory epithelium in the nasal cavity is the primary source of heat and moisture for air conditioning and contains four major cell types: basal cells; ciliated and non-ciliated columnar cells; goblet cells; and inflammatory cells (Mygind and Dahl 1998). Basal cells lie on the basement membrane serving as progenitors of other cell types and do not reach the airway lumen. Both ciliated and non-ciliated columnar cells are covered with microvilli on their apical surface. These microvilli increase the surface area of the epithelium thus facilitating exchange processes (Mygind and Dahl 1998). Compared to the submucosal glands of the nose, goblet cells contribute little to the volume of nasal secretions and little is known about their mucus release mechanisms (Beule 2010).

The respiratory mucosa is 0.3 – 5.0 mm in thickness with the thickest mucosa found on the medial aspect of the turbinates (Beule 2010). Three scroll-like turbinates (inferior, middle, and superior turbinates) originating on the lateral nasal walls project infero-medially into the airspace of the nasal cavity proper increasing the surface area/volume ratio. These turbinates divide the airspace into narrow air passages called meatuses (Moore, Agur et al. 2011). The inferior and middle turbinates are covered with respiratory epithelium while the superior turbinates are covered with olfactory epithelium. The inferior turbinate, middle turbinate, and nasal septum are underlined

by venous plexus that act as nasal erectile tissues to facilitate mucosal congestion during the nasal cycle (Cole, Haight et al. 1983, Ng, Ramsey et al. 1999, Beule 2010).

Section 3: Nasal Cycle

The nasal cycle refers to reciprocal changes in nasal airflow over a period of several hours due to alternating congestion and decongestion of the venous sinuses lining the nasal cavity, particularly on the nasal turbinates and nasal septum (Eccles 1978). The nasal cycle in its classic form maintains relatively constant total airflow (Hasegawa and Kern 1978). The nasal cycle has been reported to be present in as much as 80% of the adult population (Hasegawa and Kern 1977). The exact physiological function and the neurological control of the nasal cycle are not well understood. In many environmental or pathological situations, the nasal cycle can be modulated or even overridden (Baraniuk and Kim 2007). For example, Dallimore and Eccles found nasal resistance to decrease with physical exertion (Dallimore and Eccles 1977). The functional significance of the nasal cycle is unknown, but it is thought that the nasal cycle may play a role in respiratory defense by allowing the epithelium of the congested side to rest and recharge (Eccles 1996, Baraniuk and Kim 2007).

Section 4: Nasal Cavity Shape and Size

Respiratory conditioning is enhanced by greater contact between inspired air and the respiratory mucosa in the nasal cavity (Noback, Harvati et al. 2011). Air conditioning requirements are largely dictated by the external environment (Walker and Wells Jr 1961). Since the nasal cavity is the primary air-conditioning apparatus, it has been hypothesized that differences in nasal cavity shape across different populations are driven by adaptations to the local climate (Franciscus and

Long 1991). Specifically, these studies have shown that individuals indigenous to cold-dry environments exhibit relatively longer, taller, and narrower nasal passages than individuals from hot-humid climates (Carey and Steegmann Jr 1981, Franciscus and Long 1991, Noback, Harvati et al. 2011). These apparent climate-mediated morphologies are assumed to reflect functional differences, with longer, taller, and narrower nasal passages in cold-dry climates enhancing respiratory heat and moisture exchange via increased relative mucosal surface area (Maddux, Butaric et al. 2017). Therefore, the ratio of nasal mucosa surface area to airway volume is expected to be greater in cold-dry adapted populations than hot-humid adapted populations. Yokley (2009) makes a convincing argument for the fully decongested nose to be subject to selection pressures instead of the congested nose since the nose becomes decongested during physical exertion. Accordingly, previous studies of ecogeographic variation in nasal morphology have largely been limited to comparisons of skeletal measurements of the external nose, nasal cavity, and nasopharynx (Yokley 2009, Noback, Harvati et al. 2011, Evteev, Cardini et al. 2014, Zaidi, Mattern et al. 2017). Advances in imaging and 3D modeling capabilities now allow detailed examination of the 3D nasal anatomy including soft tissue components. Despite these advances, few studies have evaluated the contribution of soft tissues to morphological differences between cold-dry and hot-humid adapted populations. This can likely be attributed to the variable nature of nasal congestion within individuals presenting methodological challenges for 3D modeling of nasal morphology using CT imaging data (in which image data are inherently captured at a single point during the nasal cycle).

Section 5: Computational Fluid Dynamics and the Nose

Nasal physiology is closely tied to the fluid mechanical properties of the nasal airway. Since fluid mechanical properties are determined by the geometry of the flow passage, differences in nasal anatomy will result in altered function of the nose (Churchill, Shackelford et al. 2004, Naftali, Rosenfeld et al. 2005). Advances in computer resources and imaging now allow detailed analysis of airway anatomy using CT scans. Anatomically accurate 3D models created from CT scans have been used in CFD analyses to study airflow characteristics in nasal airways. CFD uses computers to simulate the flow of fluids (i.e. air) and their interactions with surfaces (Martonen, Quan et al. 2002). For the study of nasal airflow, the fluid of interest is the air.

The study of nasal airflow using CFD proceeds in the following steps: (1) CT imaging of the nasal cavity is collected; (2) Segmentation of the nasal airspace is performed to extract the fluid domain (which is synonymous with the geometry of the nasal cavity); (3) The volume occupied by the fluid (air) is divided into discrete cells (the mesh) by a process called meshing. This volume defines the space and resolution of the computer simulation; (4) Simulations are carried out and consist of equations describing the airflow, which is solved using the mesh; (5) The resulting solution is analyzed to extract useful information (Quadrio, Pipolo et al. 2014). Steps 3-5 are not unique to the study of nasal airflow, are necessary for all CFD simulations, and utilized by engineers in many applications (Quadrio, Pipolo et al. 2014).

For computer simulation of nasal airflow, the geometry of the space occupied by the fluid (air) is segmented instead of the soft tissues (which are not fluids). This space includes the air in front of the subject's face. To extract data about flow, humidity, and temperature changes of the air through the nasal cavity, the air itself must be modeled, meshed, and simulated (Quadrio, Pipolo et al. 2014).

Assessing fluid dynamics yields valuable insight into the properties of airflow in the nose and will better our understanding of the nasal physiology. However, much research to date has focused on modeling airflow in only 1-2 subjects (Jo, Chung et al. 2015, Patel, Garcia et al. 2015, de Gabory, Reville et al. 2018, Byun, Chung et al. 2019) or in subjects with pathological nasal conditions (Garcia, Bailie et al. 2007, Liu, Han et al. 2012, Patel, Garcia et al. 2015). It has been found that there is no airflow velocity in the paranasal sinuses regardless of the phase of the respiratory cycle (de Gabory et al., 2018). Few studies have compared airflow differences between populations adapted to different environments. The models and methodology developed in this practicum are being actively utilized in CFD analysis so we may examine the relationship between morphological dimensions and air conditioning capacity. In doing so, we hope to better our understanding of nasal anatomy and how it relates to nasal physiology.

SPECIFIC AIMS

Aim 1: To determine if there are significant differences in the surface area to volume (SA/V) ratio of a 3D modeled decongested vs congested nose in the same subject.

Hypothesis 1: We expect that the decongested nose of each individual will have a lower SA/V ratio than the congested nose.

Aim 2: To compare nasal cavity morphological features between subjects with European and African ancestral backgrounds.

Hypothesis 2: We expect subjects of European ancestry will exhibit significantly higher decongested SA/V ratios than subjects of African ancestry.

CHAPTER II

MATERIALS AND METHODS

Section 1: Model Creation Overview

The sample of 8 CT scans (Table 1) used in this practicum was obtained from adult patients of the Otolaryngology/Head and Neck Surgery Clinic at the University of North Carolina at Chapel Hill Hospital. CT scans had the following parameters: (1) acquisition matrix of 512 × 512 pixels, (2) pixel size of 0.3 × 0.3 mm, and (3) voxel depth of 0.7 mm. These CT scans are part of a larger collection used in a previous study by Yokley (2009) and ancestry groupings were unmodified. Though samples were not native Europeans or Africans, Yokley and Franciscus (2005) found American-based samples to be acceptable proxies for their Old-World ancestors since the groups show nasal morphology differences comparable to differences observed between supra-Saharan and sub-Saharan populations. In this previous study, Yokley assessed regional differences in internal nasal morphology using the perimeter-to-area ratio of a coronal section of the nasal cavity as a proxy for overall SA/V ratio. Yokley excluded individuals with the following from his final sample: a history of nasal surgery, excessive nasal inflammation, and obvious signs of anatomical abnormalities (i.e. excessively deviated septa, nasal polyps, major asymmetry of the nasal passages). Thus, we were confident the nasal cavities of these samples were suitable for analysis in this practicum.

TABLE 1. Sample size

Ancestry	Male	Female	Total n=8
European American	2	2	4
African American	2	2	4

Using 3D Slicer (Fedorov, Beichel et al. 2012), a model was created by first segmenting the CT scan (i.e., differentiating between cranial soft-tissues and air) in a semi-automated fashion without controlling for nasal congestion. The soft tissues were segmented first and the airway was excluded from this initial segmentation. Once the soft tissue segmentation was completed the segmentation was inverted to create a 3D model of the airspace geometry (Figure 1). The soft tissue segmentation is inverted because computer simulation of airflow requires the airspace to be modeled as a solid 3D structure (Quadrio, Pipolo et al. 2014).

FIGURE 1. Soft tissue segmentation (yellow) includes all soft tissue of the head and nasal cavity but excludes the airway. The airspace segmentation (green) excludes all soft tissue, which is unnecessary for airflow simulation. The airspace segmentation is created by inverting the soft tissue segmentation.

Section 2: Congested Model Creation

After loading the CT scan, the specimen was initially segmented using the *thresholding* tool under the *segment editor* module of 3D Slicer. The thresholding tool selects a range of greyscale values to include in the segmentation. Greyscale values in CT imaging represent x-ray beam attenuation to the tissue. Darker pixels have values closer to 0 and represent structures having less attenuation to the beam (i.e., soft tissue, air). Lighter pixels have higher values and represent structures having high attenuation (i.e., bone) (Quadrio, Pipolo et al. 2014, Athanasiou, Fotiadis et al. 2017). A thresholding level was chosen such that only soft tissue and non-airway space was included. The model was then reviewed, and the remaining paranasal sinuses were manually included in the segmentation using the *segment editor* module of 3D Slicer (Figure B1). 3D and 2D slice views (axial, coronal, sagittal) were utilized to refine the final soft tissue segmentation.

Since CFD analysis of airflow requires modeling the airspace as a single solid geometry, the soft tissue segmentation was inverted using the *logical operations* tool within the *segment editor* module. Figure 2 shows a coronal view of the segmentations before and after inversion. This inverted model represents the airspaces of the nasal cavity and the space in front of the subject's face.

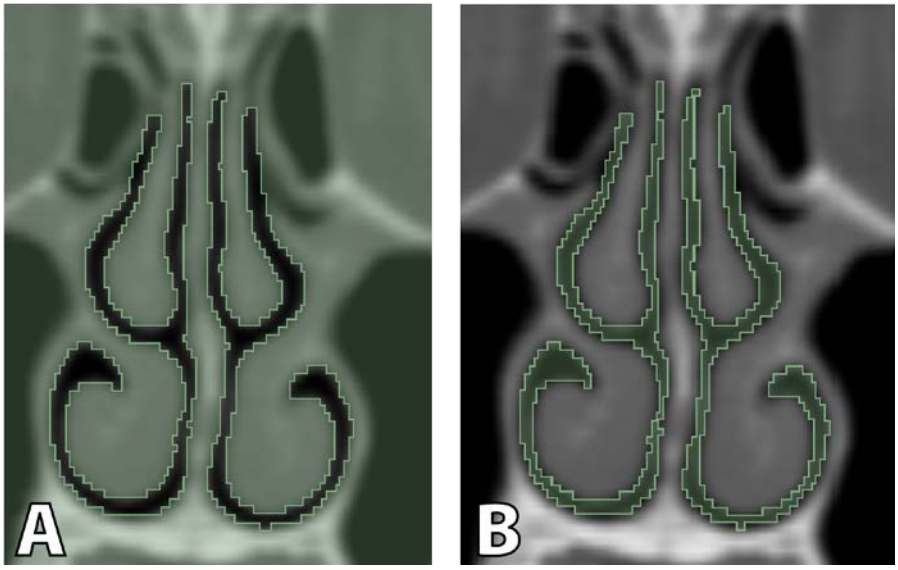

FIGURE 2. CT Coronal section. (A) soft tissue segmentation in green, (B) nasal airspace segmentation in green.

The airspace segmentation was reviewed in the 3D view to ensure there are no erroneous holes in the model (Figure 3). Once all erroneous holes were rectified, the airspace segmentation was then exported to the *models* module and saved as Standard Tessellation Language (STL) file. Using MeshMixer (AutoDesk 2017), the file size was reduced to meet the requirements for meshing. Parameters and file sizes required for meshing were set by collaborators at Dennis Lab at the University of Texas at Arlington.

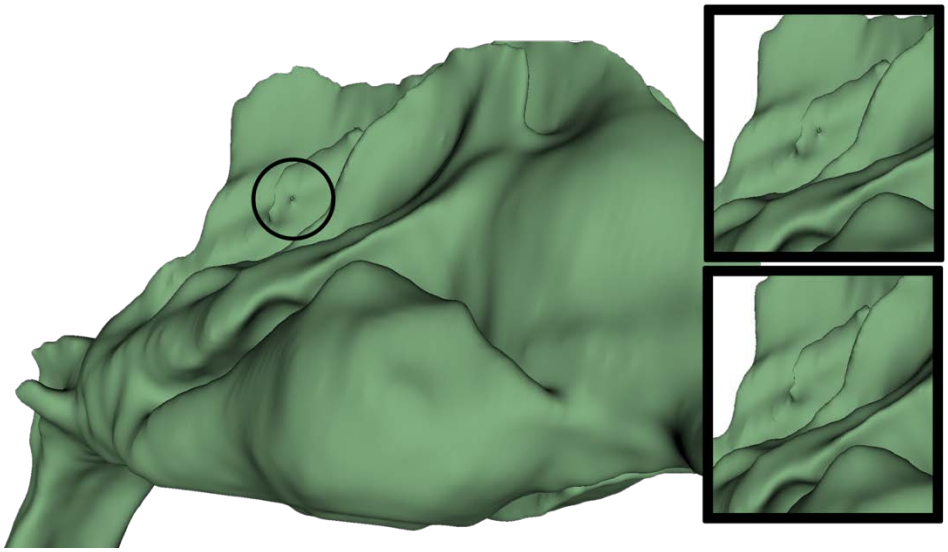

FIGURE 3. Example of erroneous hole (circled) in 3D airspace model after inversion of the soft tissue segmentation. Erroneous hole before (top) and after (bottom) correction is pictured.

Section 3: Decongested Model Creation

Using *segment editor* in 3D Slicer, an artificially decongested airway was created by reducing the erectile tissue covering the inferior turbinate, middle turbinate, and anterior septum to the level of the bone. Parts of the soft tissue that are not known to become congested were "masked" to prevent the tissues from further manipulation (e.g. bone and lateral nasal walls) (Cole, Haight et al. 1983, Ng, Ramsey et al. 1999). For instance, while decongesting the erectile tissue around the turbinates, the underlying bony turbinate was masked to prevent alteration of bony morphology.

In a new segmentation, the masks of the bony elements needed were created first (Figure 4). The bony turbinates were initially segmented using the *thresholding* tool under the *segment editor* module of 3D Slicer. A thresholding level was chosen such that only the bony turbinates

were included, and soft tissue artifacts were not tolerated (Figure 4b). Depending on the resolution of the CT scan, it was difficult to find a threshold level which included all bony elements while excluding soft tissue artifacts. Thus, the remaining segmentation of the bony turbinates and septum was manually completed. Reference segmentations of the underlying bony structure were created and employed to guide manual segmentation. Two types of reference segmentations (RS) were utilized: RS type 1 and RS type 2. RS type 1 utilized medium-tolerance thresholding where soft tissue artifacts were no larger than 1-2 pixels on coronal section (Figure 4c). RS type 2 utilized the highest-tolerance thresholding where soft tissue artifacts were larger than 2 pixels on coronal section (Figure 4d). Reference segmentations served to guide manual segmentation of the bony nasal turbinates and septum where the no-tolerance thresholding left gaps in the bony structure (Figure 4).

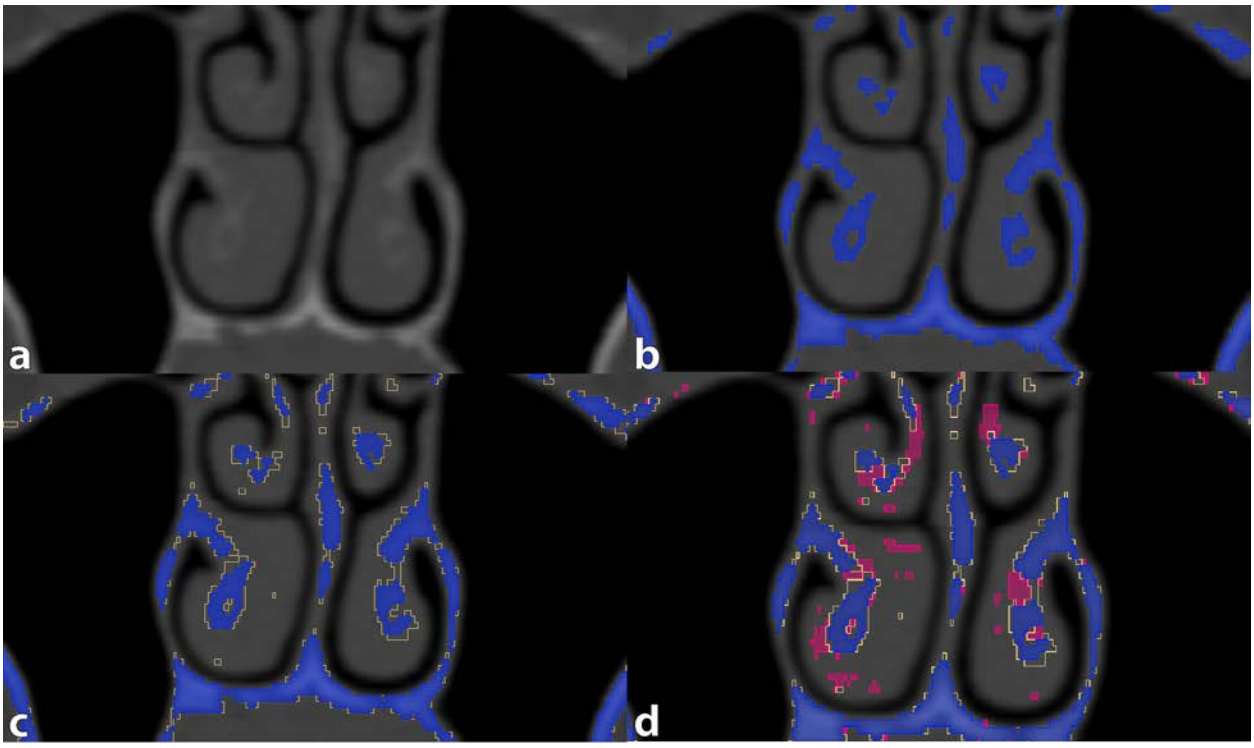

FIGURE 4. CT coronal section of the nasal cavity with bony segmentation and RS type 1 and 2 segmentations. (a) CT only, (b) bony turbinates only depicted in blue (no-tolerance thresholding, note at this level of thresholding, the bony turbinate is incomplete), (c) RS type 1 depicted in yellow outline (medium tolerance thresholding, note the soft tissue artifacts 1-2 pixels in size), (d) RS type 2 depicted in pink (highest tolerance thresholding, note the abundance of soft tissue artifacts larger than 2 pixels).

Once the bony elements underlying the nasal septum, inferior and middle turbinates were completely segmented, the soft tissue was decongested. The congested soft tissue segmentation was duplicated and was used as the basis for the decongested model. Using the completed bony segmentation, the inferior turbinate, middle turbinate, and the anterior septum containing erectile tissues were eroded to decongest the nasal cavity (Cole, Haight et al. 1983, Ng, Ramsey et al. 1999, Beule 2010). The soft tissue overlying the inferior and middle turbinates was reduced to the bony turbinates (Figure 5, right). On the septum, only the soft tissue overlying the swell body of the anterior septum was reduced (Figure 6). All other parts of the nasal cavity, such as the lateral nasal wall, were masked and protected from *in-silico* decongestion. 3D and 2D slice views (axial and coronal) were utilized in the editing process.

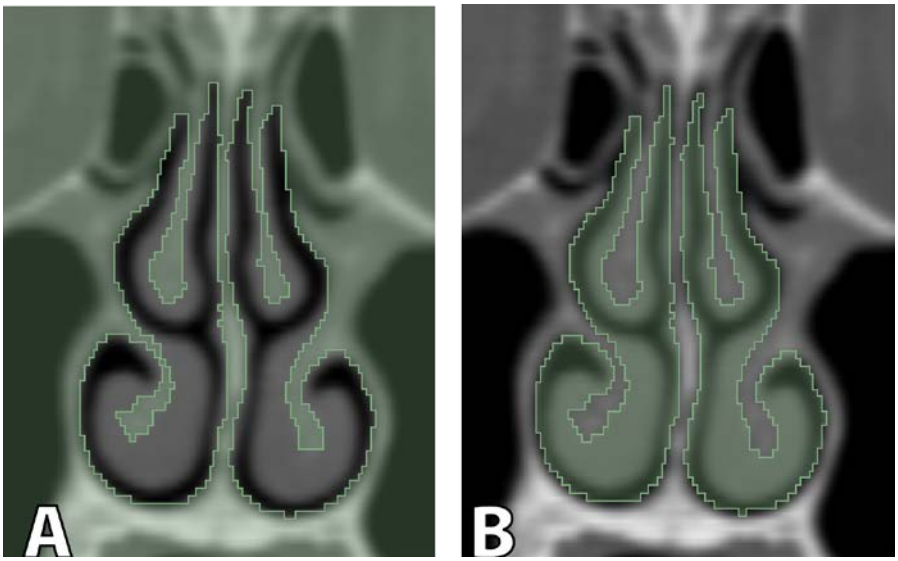

FIGURE 5. CT coronal section. Decongested soft tissue segmentation in green (left, decongested airspace segmentation in green (right).

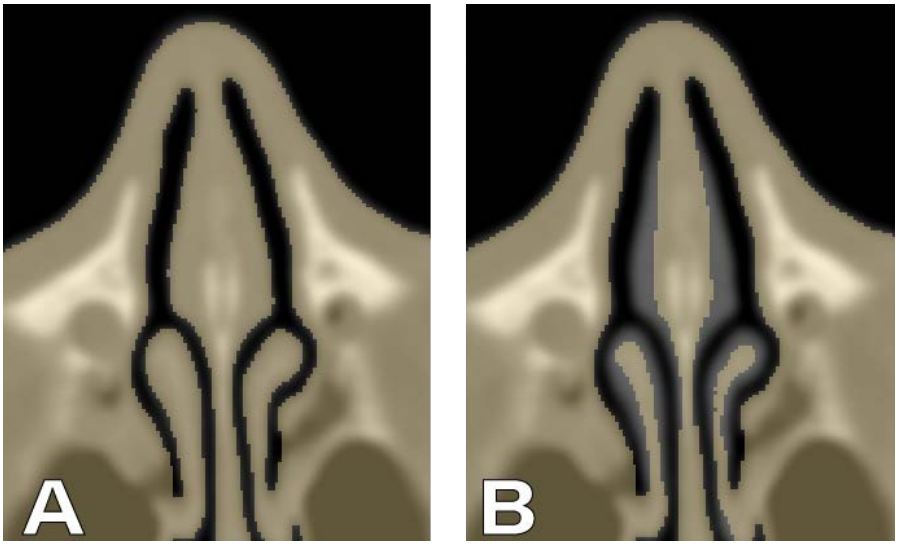

FIGURE 6. CT axial section depicting anterior septal swell body. (A) congested tissue segmentation, (B) decongested tissue segmentation

Similar to the protocol for congested models, once the decongested soft tissue segmentation was complete, a new segment layer was added, and the soft tissue segmentation was inverted using the *logical operations* tool within the *segment editor* module (Figure 5). This inverted model contained airspaces (modeled as single solid geometry) necessary for CFD analysis. The segmentation of the airspace was reviewed in the 3D view to ensure there were no erroneous holes in the model (Figure 3). Once all erroneous holes were rectified, the airspace segmentation was then exported to the *models* module and saved as a Standard Tessellation Language (STL) file. Using MeshMixer (AutoDesk 2017), the file size was reduced to meet the requirements for CFD analysis by collaborators at Dennis Lab at the University of Texas at Arlington.

Section 4: Measurements and Statistical Analysis

Volume and surface area were automatically calculated in 3D Slicer, and surface-area-to-volume ratios (SA/V) was calculated by dividing the surface area by volume. A paired t-test was used to compare SA/V ratios in congested noses versus artificially decongested noses across the entire 8 subject sample (Aim 1). The use of ratio data in these analyses was assessed by also running the same analyses on log-transformed data (which returned the identical statistical results).

Due to a small sample size, analyses of SA/V between ancestral groups (Aim 2) were performed using non-parametric two-sample t-tests (Mann Whitney U-Tests, α=0.05). Additional linear measurements (Table 2) were taken using 3D Slicer to permit evaluation of associations between SA/V ratios and overall nasal height (NH), length (NL), and width (NB) dimensions via non-parametric two-sample T-tests (Mann Whitney U-Tests, α=0.05). These measurements were taken from previous studies of internal nasal morphology (Yokley 2009, Maddux, Butaric et al. 2017, Marks, Maddux et al. 2019).

TABLE 2. Nasal passage dimensions

Measurement		Definition
NL	Nasal passage length	Anterioposterior distance between the anterior-most point of airway and staphylion (calculated from STA and AA)
NH	Internal nasal fossa height	Superioinferior distance between highest common meatus and internal nasal floor
NB	Internal nasal fossa breadth	Greatest distance between lateral nasal walls of the nasal cavity at the level of the inferior nasal turbinate (calculated from *Rns* and *Lns*)
MB	Common meatus breadth	Narrowest common meatus of the inferior nasal turbinates at NB coronal plane (calculated from *Lmb* and *Rmb*)

Section 5: Limitations

First, we acknowledge that semi-automated segmentation of CT images introduces certain variability in the resulting volumes, especially where differentiation between bone/mucosa and air was difficult. Second, we assume complete decongestion across the erectile tissue of the nose. However, it has been shown that the mucosal changes associated with the nasal cycle do not occur uniformly along the length of the nasal cavity (Abolmaali, Kantchew et al. 2013). Third, we used the level of the bone as a proxy for the fully decongested state of the inferior turbinate, middle turbinate and the anterior nasal septum. However, the mucosa of the nasal cavity is <1mm thick (Cole, Haight et al. 1983, Ng, Ramsey et al. 1999, Hadar, Yaniv et al. 2009, Beule 2010, Oltmanns, Palmowski et al. 2016).

CHAPTER III

RESULTS

Section 1: (Aim 1) Comparison of congested and decongested models.

The results of the paired t-tests support our hypothesis that the decongested nose of each individual will have a lower SA/V ratio than the congested nose. When compared to congested models, decongested models have a lower mean mucosal surface area (t=8.247, p<0.0001) and higher mean airway volume (t=-16.716, p<0.0001) resulting in lower surface-area-to-volume ratios (t=7.395, p<0.0001) (Table C2, Figure 7). Accordingly, the common meatus breadth of decongested models is also significantly larger when compared to congested models (t=-8.671, p<0.0001) (Table C2, Figure 7). Note that the values for NL, NH, and NB do not differ due to the nasal cycle, and thus, inherently exhibit no difference between congested and decongested states.

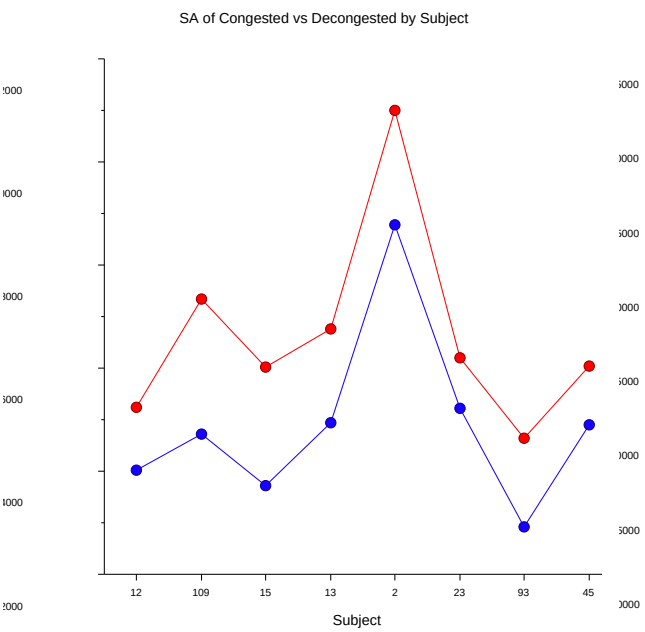

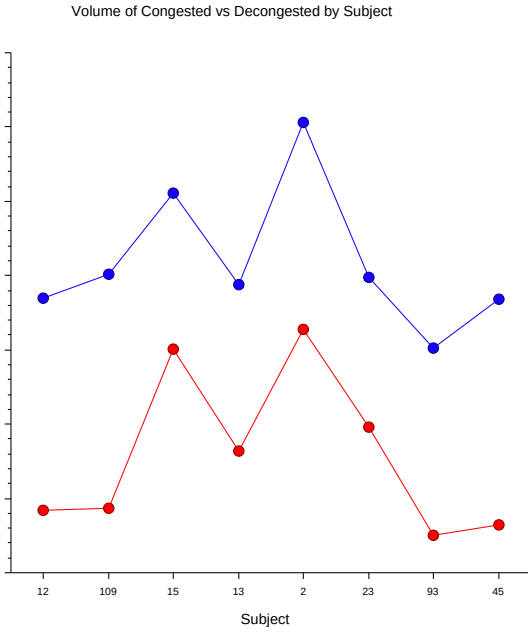

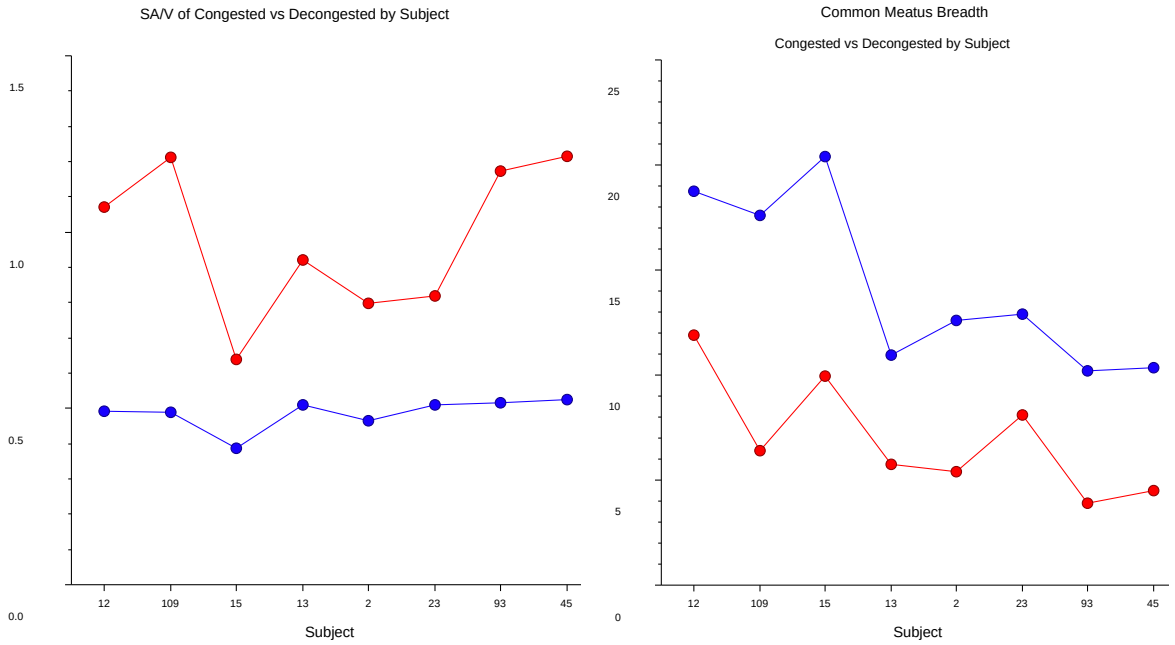

FIGURE 7. Comparison of congested (red) and decongested (blue) model measurements by subject.

Section 2: (Aim 2) Comparison of surface-area-to-volume ratios between subjects of European (EA) and African (AA) ancestral backgrounds.

The results of non-parametric two-sample t-tests (Mann Whitney U-Tests, α=0.05) were consistent with expectations. There appear to be no noticeable difference in median congested SA/V ratios (p=0.8) between EA subjects (SA/V=0.99) and AA subjects (SA/V=0.99) (Table C5, Figure 8). There was a trend for EA subjects to have greater median decongested SA/V ratios (SA/V=0.51) than AA subjects (SA/V=0.49), however, this difference did not reach statistical significance with the number of subjects included in our study (p=0.2) (Table C5, Figure 8). Further analysis reveals EA individuals' nasal length to be significantly longer than AA individuals (p=0.028) while all other measurements (NH and NB) demonstrate expected trends but are not significant (both p=0.8).

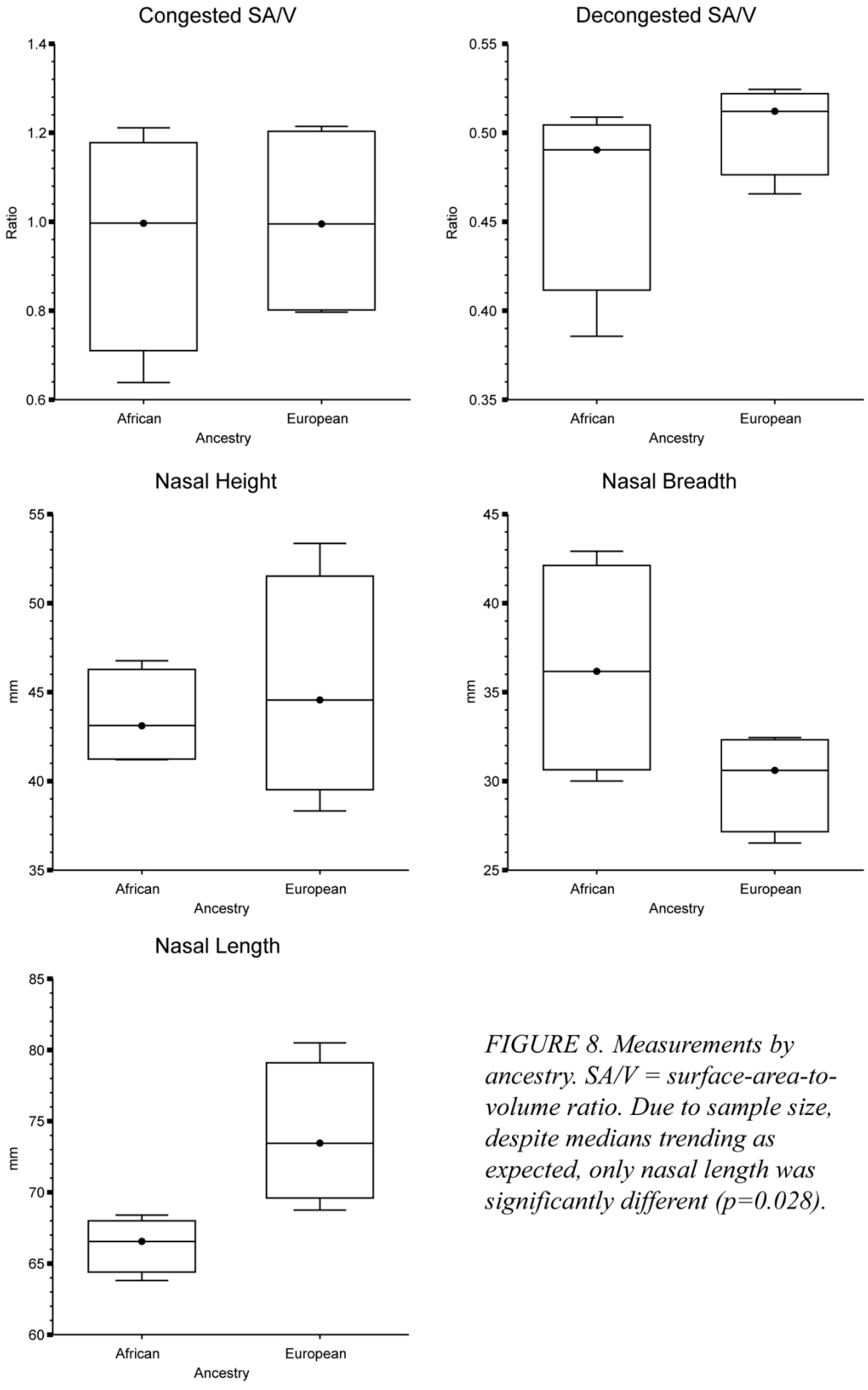

FIGURE 8. Measurements by ancestry. SA/V = surface-area-to-volume ratio. Due to sample size, despite medians trending as expected, only nasal length was significantly different (p=0.028).

CHAPTER IV

DISCUSSION

The focus of this practicum was the development of a methodology for creating realistic 3D models of the airway using Computed Tomography (CT) scans and 3D Slicer software (Fedorov, Beichel et al. 2012). The methodology developed in this practicum controls for the varied mucosal congestion of subjects captured by CT imaging by allowing *in-silico* modeling of a fully decongested nose in all individuals. The two specific aims of this study were as follows: (Aim 1) to determine whether a significant difference exists in the SA/V ratio between decongested and congested 3D models of the same subject; (Aim 2) to compare nasal cavity morphological features in subjects with European and African ancestral backgrounds.

Our results show that *in-silico* decongestion of the nasal cavity had significant impacts on MB, SA, V, and SA/V ratios when compared to the congested models in the same individual, thus supporting our hypothesis for Aim 1. Among decongested models, SA and SA/V were consistently lower in every individual. Similarly, V was consistently higher, and MB was consistently wider in all individuals. Numerous CFD analyses of airflow demonstrate that the geometry of the flow passage (i.e. the nasal cavity) significantly impacts the resulting flow (Churchill, Shackelford et al. 2004, Naftali, Rosenfeld et al. 2005, Liu, Han et al. 2012, Yu, Shademan et al. 2012). As such, our results provide evidence that differential levels of non-pathological mucosal congestion between subjects (related to the nasal cycle) could significantly impact CT imaging-based

morphometric analyses of nasal cavity anatomy, and consequently, any subsequent CFD analyses of nasal airflow based on congested airway models.

Importantly, the nasal cycle is rarely controlled prior to CT imaging (e.g. by the administration of nasal decongestant sprays), likely resulting in CT scans imaging subjects at different phases of the cycle. Further, it has been suggested that up to 20% of adults may not exhibit a nasal cycle (Hasegawa and Kern 1977), further contributing to population-level variation in nasal soft-tissue and airway anatomy. Cumulatively, the results of this study thus highlight the importance of controlling for nasal congestion prior to evaluating the contributions of soft tissues to morphological differences between cold-dry adapted populations and hot-humid adapted populations.

For Aim 2, there was a trend for EA individuals to have higher decongested median SA/V ratios than AA individuals, but this trend was not statistically significant with the small number of subjects included in our study. The observed trend was similar to a significant finding by Yokley (2009). Using perimeter-to-area (P/A) ratios as a proxy for SA/V ratios, Yokley (2009) demonstrated that decongested AA individuals had significantly lower P/A ratios relative to decongested EA individuals. These trends in P/A ratios are consistent with the hypothesized need for increased SA/V ratio due to increased physiological demand for air conditioning in cold-dry climates. Our results extend Yokley's (2009) finding, strongly suggesting that similar trends in ecogeographic variation will be observed in SA/V ratios of indigenous populations from extremely cold-dry (e.g., Arctic Circle) and hot-humid (e.g., Equatorial rainforest) environments.

Further analysis compared linear measurements of nasal height (NH), nasal breadth (NB), common meatus breadth (MB), and nasal length (NL) between EA and AA individuals. Though not significant due to a small sample, EA individuals tended to have taller median NH, narrower

median NB, and narrower MB (congested and decongested) than AA individuals. EA individuals were found to possess significantly longer nasal passages (NL) than AA individuals. These trends are consistent with trends observed in the literature (Franciscus and Long 1991), with cold-dry adapted populations exhibiting taller, longer, and narrower nasal passages than hot-humid adapted populations.

Since measurements of NL included the external nose, this result is consistent with previous studies of nasal protrusion (Carey and Steegmann Jr 1981, Franciscus and Trinkaus 1988). Churchill et al., (2004) suggests that nasal protrusion may play some role in increasing air conditioning capacity by increasing heat and moisture exchange. Whether it increases air conditioning capacity by increasing turbulence, increasing SA, or both is yet to be known. Future studies involving CFD analysis of nasal airflow can elucidate the role of nasal protrusion in evolutionary adaptation.

These methods for *in-silico* decongestion of the nose are being actively employed to quantify the nasal cavity morphologies of subjects of European and African ancestral backgrounds. The models and methods developed in this practicum are also being utilized to generate 3D models of the nasal cavity for CFD analysis in conjunction with our collaborators at Dennis lab at the University of Texas at Arlington. Ongoing research employing CFD analyses will hopefully provide insight into how morphological differences impact intranasal heat and moisture exchange thus providing further insight into how ecogeographic variation in human nasal morphology may reflect climatically adaptive differences in nasal function.

CHAPTER V

SUMMARY AND CONCLUSIONS

This study examined human nasal morphology using 3D modeling. Previous research has mostly focused on the morphology of the nasal skeleton with little consideration of the nasal soft tissues (e.g., cartilage, mucosa) (Franciscus and Long 1991, Noback, Harvati et al. 2011, Evteev, Cardini et al. 2014). Other research to date has focused on modeling airflow in only 1-2 subjects (Jo, Chung et al. 2015, Patel, Garcia et al. 2015, de Gabory, Reville et al. 2018, Byun, Chung et al. 2019) or in subjects with pathological nasal conditions (Garcia, Bailie et al. 2007, Liu, Han et al. 2012, Patel, Garcia et al. 2015). This study developed methodological protocols to control for variable mucosal congestion (both due to and independent of the nasal cycle).

For Aim 1, we hypothesized that the decongested nose of each individual would have a lower SA/V ratio than the congested nose. As expected, SA/V was significantly lower after *in-silico* decongestion for each individual across all individuals.

For Aim 2, we hypothesized EA individuals would exhibit higher SA/V ratios that AA individuals upon *in-silico* decongestion. We expected no difference in congested SA/V ratios between EA or AA individuals. As expected, there was no difference between congested SA/V ratios between EA or AA individuals. Although not significant, we observed a general trend for EA individuals to have greater decongested SA/V ratios than AA individuals. Further analysis revealed EA individuals to possess significantly longer nasal passages than AA individuals.

Similarly, though not significant due to a small sample, EA individuals also tended to exhibit narrower NB and taller NH values than AA individuals.

In conclusion, this study has demonstrated the importance of controlling for variable nasal congestion when evaluating nasal passages since the geometry of the nasal passages, their fluid mechanical properties, and the resulting physiology are inextricably linked (Churchill, Shackelford et al. 2004, Naftali, Rosenfeld et al. 2005). In the future, studies should employ larger sample sizes in order to detect significant differences between EA and AA individuals. Furthermore, the present study will continue as a part of a larger project investigating the nasal cavity using 3D modeling. The 3D models of the nasal cavity created in this study are currently being employed in CFD analysis of nasal airflow to expand our understanding of ecogeographic patterning and how it may relate to nasal airflow dynamics.

CHAPTER VII

INTERNSHIP EXPERIENCE

DESCRIPTION OF INTERNSHIP SITE AND EXPERIENCE

This internship practicum was performed at the University of North Texas Health Science Center in Fort Worth, TX, under the direct supervision of Scott Maddux, Ph.D., over the course of one year as a partial requirement for the degree of Master of Science in Medical Sciences. In May 2019, I transferred to the Medical Sciences Research Track program. From May 2019 to September 2019, I submitted primary and secondary applications to numerous medical schools for entry year 2020. In August of 2019, Dr. Maddux accepted my transfer into his lab and introduced me to this project and his previous work. From August 2019 through September 2019, Dr. Maddux and I held weekly meetings to discuss previous research and literature to build a foundation upon which I would build this project. In September 2019, alongside the first-year students of the Texas College of Osteopathic Medicine (TCOM), I completed Head and Neck Anatomy. The course included gross laboratory dissections and lecture-based learning. In early December 2019, I presented my practicum research proposal as a "Work-in-Progress" (WIP) seminar in the Center for Anatomical Sciences.

The sample of CT scans utilized in this study were originally used in Dr. Todd Yokley's 2009 study. They were assembled from adult patients of the Otolaryngology/Head and Neck Surgery Clinic at the University of North Carolina at Chapel Hill Hospital. I gained basic 3D Slicer proficiency using the tutorials and manuals offered by 3D Slicer and by Dr. Lauren Butaric. In

October 2019, I met with Dennis Lab, my collaborators, at the University of Texas at Arlington to gain an understanding on the model requirements for computational fluid dynamics (CFD) analysis of nasal air flow. As the focus of the practicum is methodology, from October through February 2020, I focused on developing methodology to artificially decongest human nasal cavities from CT scans using 3D Slicer. From January 2019 to March 2019 Decongested models of the nasal airway were sent to collaborators for CFD analyses at Dennis Lab as they were completed.

Upon completion of data acquisition, interlandmark distances, surface area, and volumes were calculated and analyzed with Dr. Maddux. The results of which have been reported in this practicum report. An abstract of the work done in part by this practicum, and by collaborators at Dennis Lab, was accepted for the 2020 UNTHSC Research Appreciation Day (March 27, 2020). An abstract was also accepted for a poster presentation at Experimental Biology 2020 in San Diego, California and publication in the FASEB journal. Finally, I will be presenting the results at the 2020 JPS Symposium in Fort Worth, Texas (June 5, 2020).

This internship introduced me to the rigorous field of graduate-level research and has helped me grow as a scientist. I am thankful for the mentorship of Dr. Maddux and Dr. Menegaz. I look forward to continuing my work as a part of the TCOM class of 2024.

APPENDIX A

ABBREVIATIONS

TABLE A1: List of abbreviations

Abbreviation	Explanation
AA	African American
CFD	Computational Fluid Dynamics
CT	Computed Tomography
EA	European American
MB	Common meatus breadth
NB	Nasal breadth
NH	Nasal height
NI	Nasal index
NL	Nasal length
RS	Reference Segmentation
SA	Surface Area
SA/V	Surface-Area-to-Volume Ratio
STL	Standard Tessellation Language (file type)
V	Volume

APPENDIX B

METHODOLOGY ILLUSTRATIONS

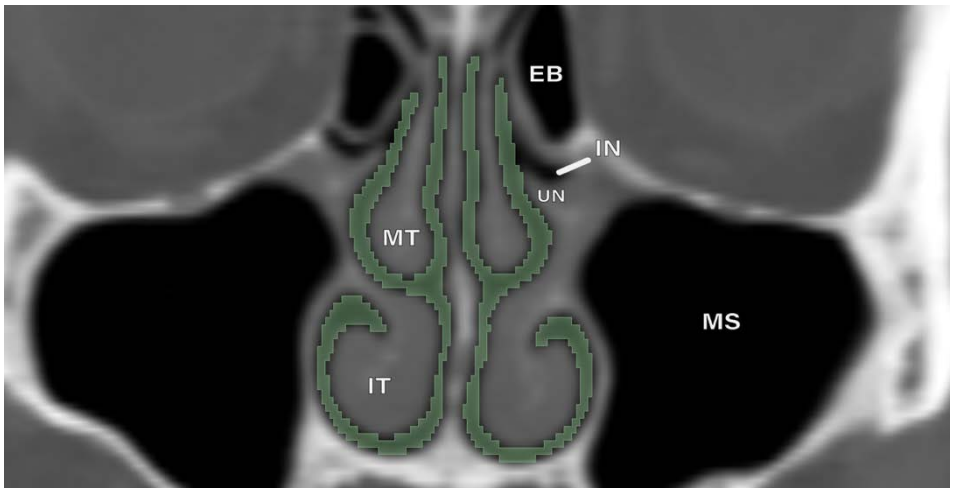

FIGURE B1. Example of paranasal sinus exclusion from airway model on CT coronal section. This image shows the uncinate process (UN) as border to exclude the infundibulum (IN). MS=maxillary sinus, IT=inferior turbinate, MT=middle turbinate, EB=ethmoid bullae.

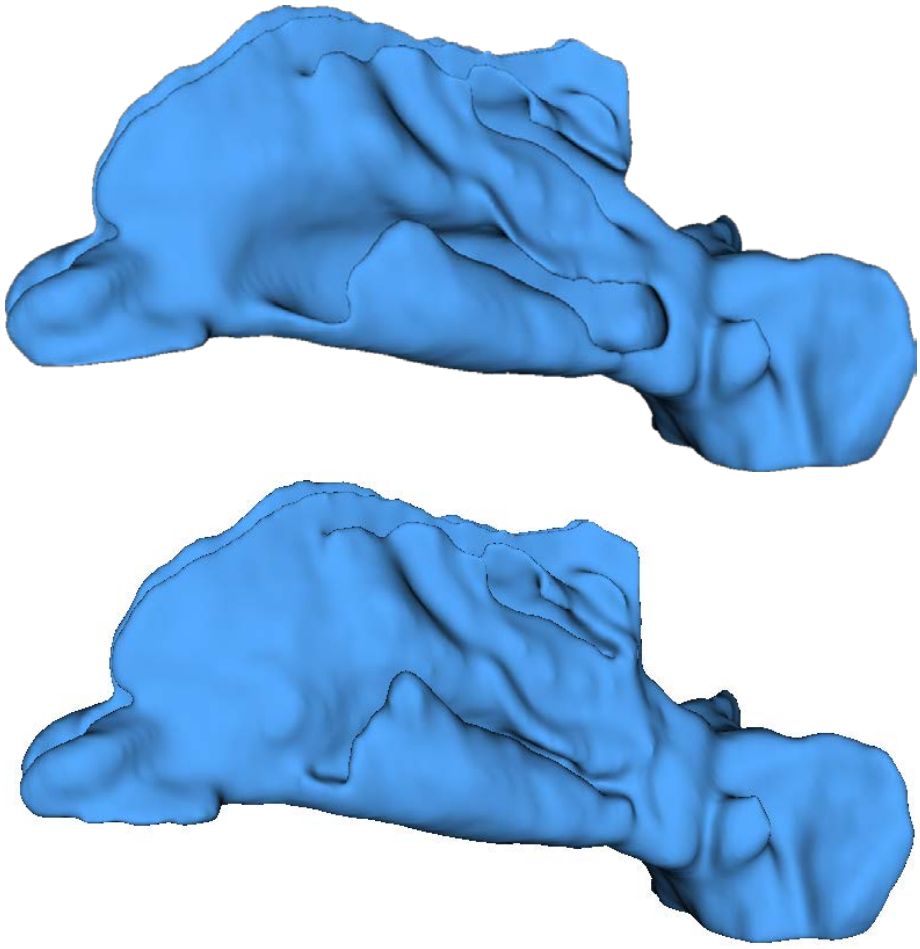

FIGURE B2. Completed 3D models of nasal airspace. Congested (top). Decongested (bottom).

APPENDIX C

SUBJECT DATA AND RESULTS

TABLE C1. Means and standard deviations of surface area (SA), volume (V), ratios (SA/V), and common meatus breadth (MB)

	Congested	Decongested	*T*	*p*-value
SA	16653.12 mm^2 (1942.13)	14902.45 mm^2 (1742.78)	8.2475	<0.0001*
V	17955.1 mm^3 (5404.97)	30911.5 mm^3 (4788.42)	-16.7163	<0.0001*
SA/V	0.98 (0.22)	0.48 (0.04)	7.3957	<0.0001*
MB	6.99 mm (2.78)	14.22 mm (4.07)	-8.6711	<0.0001*

Values within parentheses indicate the standard deviation.
*Indicates significant difference (α=0.05)

TABLE C2. Surface area, volume, and ratios of each subject before and after in-silico decongestion

			Congested			Decongested		
	Sex	Ancestry	SA	V	SA/V	SA	V	SA/V
002	M	EA	20993.73	26351.6	0.79	18776.83	40335.7	0.46
023	M	EA	16208.59	19820.7	0.81	15215.17	29881.5	0.50
045	F	EA	16032.69	13206.7	1.21	14904.27	28429.5	0.52
093	F	EA	14642.36	12488.8	1.17	12919.84	25086.4	0.51
013	M	AA	16758.16	18196.3	0.92	14949.32	29392.6	0.50
015	M	AA	16019.00	25062.9	0.63	13721.35	35570.6	0.38
012	F	AA	15230.36	14205.9	1.07	14013.44	28487.9	0.49
109	F	AA	17340.09	14308.2	1.21	14719.39	30107.9	0.48

EA= European American, AA= African American, SA=surface area (mm^2), V=volume (mm^3), SA/V= surface-area-to-volume ratio

TABLE C3. Nasal passage measurements and the nasal index by subject

						MB		
	Sex	Ancestry	NL	NH	NB	Decongested	Congested	NI
002	M	EA	80.50 mm	53.36 mm	32.43 mm	12.61 mm	5.41 mm	60.7
023	M	EA	74.79 mm	43.19 mm	29.17 mm	12.91 mm	8.10 mm	67.5
045	F	EA	68.73 mm	45.92 mm	32.0 mm	10.34 mm	4.50 mm	69.7
093	F	EA	72.12 mm	38.30 mm	26.51 mm	10.20 mm	3.91 mm	69.2
013	M	AA	68.38 mm	46.75 mm	30.00 mm	10.9 mm	5.75 mm	64.1
015	M	AA	66.29 mm	41.19 mm	39.76 mm	20.40 mm	9.97 mm	96.5
012	F	AA	63.79 mm	41.31 mm	32.57 mm	18.75 mm	11.88 mm	78.8
109	F	AA	66.81 mm	44.90 mm	42.91 mm	17.58 mm	6.38 mm	95.5

NL = nasal length, NH= nasal height, NB= nasal breadth, MB= common meatus breadth, NI= nasal index (NB/NH)×100

TABLE C4. Mean and median surface areas (SA), volumes (V), and ratios (SA/V) by ancestry

	European American		African American		
	Mean	Median	Mean	Median	*p*-value
Congested					
SA	16969.34 mm^2 (2772.88)	16120.64 mm^2	16336.90 mm^2 (914.57)	16388.58 mm^2	1.000
V	17966.95 mm^3 (6491.24)	16513.70 mm^3	17943.32 mm^3 (5096.88)	16252.25 mm^3	0.885
SA/V	1.00 (0.22)	0.99	0.96 (0.24)	0.99	0.885
Decongested					
SA	15454.03 mm^2 (2437.37)	15059.72 mm^2	14350.88 mm^2 (578.53)	14366.42 mm^2	0.485
V	30933.28 mm^3 (6581.96)	29155.50 mm^3	30889.75 mm^3 (3190.19)	29750.25 mm^3	0.685
SA/V	0.50 (0.02)	0.51	0.46 (0.05)	0.49	0.200

Values within parentheses indicate the standard deviation.

TABLE C5. Nasal length (NL), nasal height (NH), nasal breadth (NB) by ancestry

	European American		African American		
	Mean	Median	Mean	Median	*p*-value
NL	74.03mm (4.97)	73.45 mm	66.32 mm (1.90)	66.55 mm	0.028*
NH	45.19 mm (6.29)	44.56 mm	43.54 mm (2.74)	43.11 mm	0.885
NB	30.03 mm (2.76)	30.60 mm	36.31 mm (6.03)	36.17 mm	0.885

Values within parentheses indicate the standard deviation.
*Indicates significant difference

TABLE C6. Common meatus breadth (MB) and nasal index (NI) by ancestry

	European American		African American		
	Mean	Median	Mean	Median	*p*-value
MB					
Congested	5.48 mm (1.85)	4.95 mm	8.50 mm (2.92)	8.17 mm	0.114
Decongested	11.52 mm (1.44)	11.47 mm	16.92 mm (4.15)	18.16 mm	0.114
NI					
Max	66.81 (4.13)	68.36	83.77 (15.38)	87.20	0.200
Min	25.67 (3.31)	25.13	39.37 (11.46)	42.27	0.200

Values within parentheses indicate the standard deviation. NI max = (NB/NH)×100; NI min = (NB/decongested MB)×100

APPENDIX D

LANDMARKS

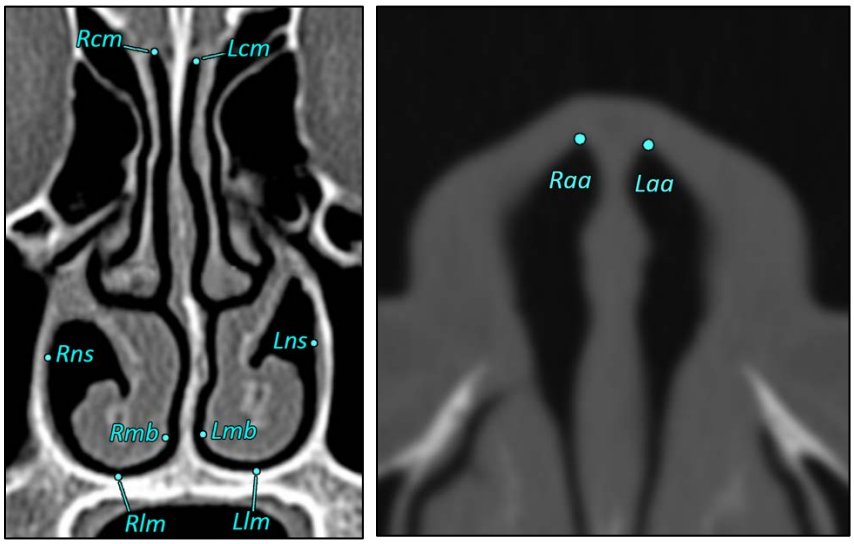

FIGURE D1. Landmarks taken on coronal (left) and axial (right) CT section

TABLE D1. List of landmarks

Landmark		Definition
HCM	Highest common meatus	Midpoint of *Rcm* and *Lcm*
Rcm	Right highest common meatus	Highest point of right common meatus at the highest point of nasal cavity roof
Lcm	Left highest common meatus	Highest point of left common meatus at the highest point of the nasal cavity roof
INF	Internal nasal floor	Midpoint of *Rlm* and *Llm*
Rlm	Right internal nasal floor	Lowest point on the nasal floor of the right nasal cavity below HCM
Llm	Left internal nasal floor	Lowest point on the nasal floor of the left nasal cavity below HCM
Rns	Right nasal side wall	Right nasal side wall at the widest breath of the internal nose
Lns	Left nasal side wall	Left nasal side wall at the widest breath of the internal nose
Lmb	Left medial turbinate	Medial part of left inferior turbinate at the widest breadth of the internal nose on coronal CT section
Rmb	Right medial turbinate	Medial part of right inferior turbinate at the widest breadth of the internal nose on coronal CT section
AMA	Anterior-most point of airway	Midpoint of *Raa* and *Laa*
Raa	Right anterior-most airway	Anterior-most point of right airway on axial CT section
Laa	Left anterior-most airway	Anterior-most point of left airway on axial CT section
STA	Staphylion	Midpoint of *Rpnf* and *Lpnf*
Rpnf	Right posterior nasal floor	Right posterior edge of hard palate
Lpnf	Left posterior nasal floor	Left posterior edge of hard palate

BIBLIOGRAPHY

Abolmaali, N., A. Kantchew and T. Hummel (2013). "The nasal cycle: Assessment using MR imaging." Chemosensory Perception **6**(3): 148-153.

Athanasiou, L. S., D. I. Fotiadis and L. K. Michalis (2017). 2 - Principles of Coronary Imaging Techniques. Atherosclerotic Plaque Characterization Methods Based on Coronary Imaging. L. S. Athanasiou, D. I. Fotiadis and L. K. Michalis. Oxford, Academic Press**:** 23-47.

AutoDesk (2017). MeshMixer, AutoDesk**:** Computer Software.

Baraniuk, J. N. and D. Kim (2007). "Nasonasal reflexes, the nasal cycle, and sneeze." Current Allergy and Asthma Reports **7**(2): 105-111.

Beule, A. G. (2010). "Physiology and pathophysiology of respiratory mucosa of the nose and the paranasal sinuses." GMS Curr Top Otorhinolaryngol Head Neck Surg **9**: Doc07.

Butaric, L. N. and S. D. Maddux (2016). "Morphological Covariation between the Maxillary Sinus and Midfacial Skeleton among Sub-Saharan and Circumpolar Modern Humans." American Journal of Physical Anthropology **160**(3): 483-497.

Byun, S., S. K. Chung and Y. Na (2019). "Air-conditioning characteristics in nasal cavity models exhibiting nasal cycle states." Journal of Thermal Biology **83**: 60-68.

Carey, J. W. and A. T. A. T. Steegmann Jr (1981). "Human nasal protrusion, latitude, and climate." American Journal of Physical Anthropology **56**(3): 313-319.

Churchill, S. E., L. L. Shackelford, J. N. Georgi and M. T. Black (2004). "Morphological variation and airflow dynamics in the human nose." Am J Hum Biol **16**(6): 625-638.

Cole, P., J. S. Haight, P. W. Cooper and E. E. Kassel (1983). "A computed tomographic study of nasal mucosa: effects of vasoactive substances." J Otolaryngol **12**(1): 58-60.

Dallimore, N. S. and R. Eccles (1977). "Changes in human nasal resistance associated with exercise, hyperventilation and rebreathing." Acta Oto-Laryngologica **84**(1-6): 416-421.

de Gabory, L., N. Reville, Y. Baux, N. Boisson and L. Bordenave (2018). "Numerical simulation of two consecutive nasal respiratory cycles: toward a better understanding of nasal physiology." Int Forum Allergy Rhinol **8**(6): 676-685.

Eccles, R. (1978). "The central rhythm of the nasal cycle." Acta Oto-Laryngologica **86**(5-6): 464-468.

Eccles, R. (1996). "A role for the nasal cycle in respiratory defence." Eur Respir J **9**(2): 371-376.

Evteev, A., A. L. Cardini, I. Morozova and P. O'Higgins (2014). "Extreme climate, rather than population history, explains mid-facial morphology of Northern Asians." American Journal of Physical Anthropology **153**(3): 449-462.

Fedorov, A., R. Beichel, J. Kalpathy-Cramer, J. Finet, J.-C. Fillion-Robin, S. Pujol, C. Bauer, D. Jennings, F. Fennessy, M. Sonka, J. Buatti, S. Aylward, J. V. Miller, S. Pieper and R. Kikinis (2012). "3D Slicer as an image computing platform for the Quantitative Imaging Network." Magnetic resonance imaging **30**(9): 1323-1341.

Franciscus, R. G. and J. C. Long (1991). "Variation in human nasal height and breadth." American Journal of Physical Anthropology **85**(4): 419-427.

Franciscus, R. G. and E. Trinkaus (1988). "Nasal morphology and the emergence of Homo erectus." American Journal of Physical Anthropology **75**(4): 517-527.

Garcia, G. J. M., N. Bailie, D. A. Martins and J. S. Kimbell (2007). "Atrophic rhinitis: A CFD study of air conditioning in the nasal cavity." Journal of Applied Physiology **103**(3): 1082-1092.

Hadar, T., E. Yaniv, Y. Shvili, R. Koren and J. Shvero (2009). "Histopathological changes of the nasal mucosa induced by smoking." Inhal Toxicol **21**(13): 1119-1122.

Hasegawa, M. and E. B. Kern (1977). "The human nasal cycle." Mayo Clin Proc **52**(1): 28-34.

Hasegawa, M. and E. B. Kern (1978). "The effect of breath holding, hyperventilation, and exercise on nasal resistance." Rhinology **16**(4): 243-249.

Jo, G., S. K. Chung and Y. Na (2015). "Numerical study of the effect of the nasal cycle on unilateral nasal resistance." Respiratory Physiology and Neurobiology **219**: 58-68.

Liu, T., D. Han, J. Wang, J. Tan, H. Zang, T. Wang, Y. Li and S. Cui (2012). "Effects of septal deviation on the airflow characteristics: using computational fluid dynamics models." Acta Otolaryngol **132**(3): 290-298.

Maddux, S. D., L. N. Butaric, T. R. Yokley and R. G. Franciscus (2017). "Ecogeographic variation across morphofunctional units of the human nose." American Journal of Physical Anthropology **162**(1): 103-119.

Marks, T. N., S. D. Maddux, L. N. Butaric and R. G. Franciscus (2019). "Climatic adaptation in human inferior nasal turbinate morphology: Evidence from Arctic and equatorial populations." American Journal of Physical Anthropology **169**(3): 498-512.

Martonen, T. B., L. Quan, Z. Zhang and C. J. Musante (2002). "Flow simulation in the human upper respiratory tract." Cell Biochem Biophys **37**(1): 27-36.

Moore, K. L., A. M. R. Agur and A. F. Dalley (2011). Essential clinical anatomy. Baltimore, MD, Lippincott Williams & Wilkins.

Mygind, N. and R. Dahl (1998). "Anatomy, physiology and function of the nasal cavities in health and disease." Advanced Drug Delivery Reviews **29**(1-2): 3-12.

Naftali, S., M. Rosenfeld, M. Wolf and D. Elad (2005). "The air-conditioning capacity of the human nose." Annals of Biomedical Engineering **33**(4): 545-553.

Ng, B. A., R. G. Ramsey and J. P. Corey (1999). "The distribution of nasal erectile mucosa as visualized by magnetic resonance imaging." Ear, Nose and Throat Journal **78**(3): 159-166.

Noback, M. L., K. Harvati and F. Spoor (2011). "Climate-related variation of the human nasal cavity." American Journal of Physical Anthropology **145**(4): 599-614.

Oltmanns, U., K. Palmowski, M. Wielpütz, N. Kahn, E. Baroke, R. Eberhardt, S. Wege, M. Wiebel, M. Kreuter, F. J. F. Herth and M. A. Mall (2016). "Optical coherence tomography detects structural abnormalitiesof the nasal mucosa in patients with cystic fibrosis." Journal of Cystic Fibrosis **15**(2): 216-222.

Patel, R. G., G. J. M. Garcia, D. O. Frank-Ito, J. S. Kimbell and J. S. Rhee (2015). "Simulating the nasal cycle with computational fluid dynamics." Otolaryngology - Head and Neck Surgery (United States) **152**(2): 353-360.

Quadrio, M., C. Pipolo, S. Corti, R. Lenzi, F. Messina, C. Pesci and G. Felisati (2014). "Review of computational fluid dynamics in the assessment of nasal air flow and analysis of its limitations." Eur Arch Otorhinolaryngol **271**(9): 2349-2354.

Walker, J. E. C. and R. E. Wells Jr (1961). "Heat and water exchange in the respiratory tract." Amer. J. Med. **30**(2): 259-267.

Yokley, T. R. (2009). "Ecogeographic variation in human nasal passages." American Journal of Physical Anthropology **138**(1): 11-22.

Yokley, T. R. and R. G. Franciscus (2005). "Variation in Nasal Passage Surface-Area-to-Volume Ratios of Recent and Fossil Humans." Abstracts of the PaleoAnthropology Society 2005 Meetings **A12**.

Yu, Y., M. Shademan, R. Balachandar and R. Barron (2012). "CFD Study of Effects of Geometry Variations on Flow in a Nozzle." Engineering Applications of Computational Fluid Mechanics **6**: 412.

Zaidi, A. A., B. C. Mattern, P. Claes, B. McEvoy, C. Hughes and M. D. Shriver (2017). "Investigating the case of human nose shape and climate adaptation." PLoS Genet **13**(3): e1006616.